

Development of a New Far Infrared Laser Interferometer in Heliotron J and First Results

Yoshiaki OHTANI, Shinsuke OHSHIMA¹⁾, Nuttasart ASAVATHAVORNVANIT, Tsuyoshi AKIYAMA²⁾, Takashi MINAMI¹⁾, Kenji TANAKA²⁾, Kazunobu NAGASAKI¹⁾, Nan SHI³⁾, Tohru MIZUUCHI¹⁾, Nikolai. B. MARUSHCHENKO⁴⁾, Shinji KOBAYASHI¹⁾, Hiroyuki OKADA¹⁾, Shinnichiro KADO¹⁾, Satoshi YAMAMOTO¹⁾, Linge ZANG¹⁾, Gavin M. WEIR¹⁾, Naoki KENMOCHI, Shigeru KONOSHIMA¹⁾, Yuji NAKAMURA, Yuriy TURKIN⁴⁾ and Fumimichi SANO¹⁾

Graduate School of Energy Science, Kyoto University, Gokasho, Uji 611-0011, Japan

¹⁾*Institute of Advanced Energy, Kyoto University, Gokasho, Uji 611-0011, Japan*

²⁾*National Institute for Fusion Science, 322-6 Oroshi-cho, Toki 509-5292, Japan*

³⁾*Institute of Plasma Physics, Chinese Academy of Sciences, Hefei, Anhui, 230031, P.R. China*

⁴⁾*Max-Planck-Institute for Plasma Physics, Wendelsteinstraße 117491 Greifswald, German*

(Received 9 February 2015 / Accepted 1 September 2015)

A new far infrared (FIR) laser interferometer with high time resolution has been developed in Heliotron J for measuring high performance plasmas. The FIR laser interferometer is a heterodyne-type Michelson interferometer with a 1 MHz intermediate frequency. The interferometer uses a super rotating grating and the viewing chord passes through an off-axis position. Refraction in high density plasma is estimated using the TRAVIS ray-tracing code. The results suggest that it is possible to extend the range of the interferometer up to $1.5 \times 10^{20} \text{ m}^{-3}$. The first line-averaged plasma density measurements using the FIR laser interferometer have been made in ECH and NBI heated plasmas. The relative change in the density profile shape is evaluated from the ratio of the line-averaged density obtained by the FIR laser and microwave interferometer with a different viewing chord. The difference in the measurements suggests that a more peaked density profile is formed in NBI plasma than in ECH + NBI plasma, which is in agreement with Nd:YAG Thomson scattering measurements.

© 2015 The Japan Society of Plasma Science and Nuclear Fusion Research

Keywords: FIR interferometer, plasma diagnostics, electron density, helical device, Heliotron

DOI: 10.1585/pfr.10.1402091

1. Introduction

High-density plasma production using advanced fueling techniques is needed to realize controlled thermonuclear fusion and is of interest to plasma physics. In the Large Helical Device, super dense core plasma with an internal diffusion barrier has been observed in pellet injection experiments with an actively pumped local island divertor. This demonstrates the possibility of relatively low-temperature and high density operation in helical reactors [1, 2]. In the helical axis heliotron device, Heliotron J, supersonic molecular beam injection (SMBI) has improved plasma performance and expanded the plasma density range up to approximately $5 \times 10^{19} \text{ m}^{-3}$ with a stored energy of approximately 4.5 kJ [3]. In recent years, plasma densities greater than $1 \times 10^{20} \text{ m}^{-3}$ have been produced by combining a low toroidicity configuration with high-intensity gas-puff (HIGP) fueling [4].

To measure the plasma electron density, a new far infrared (FIR) laser interferometer has been developed in Heliotron J. The specifications of the interferometer are

as follows: (i) the observable electron density range is $1 \times 10^{18} - 1.5 \times 10^{20} \text{ m}^{-3}$, (ii) the time resolution is less than 1 μs , and (iii) the beam diameter is less than 30 mm.

The design of the new FIR interferometer in Heliotron J considered laser refraction in high density plasma using the TRAVIS ray-tracing code [5], and is discussed in Sec. 2. In Sec. 3, the first results with the laser interferometer are discussed and compared with the results of the microwave interferometer.

2. Experimental Setup

2.1 FIR interferometer

An HCN laser ($\lambda = 337 \mu\text{m}$) [6] was chosen as the light source to measure plasma with line-averaged density of $1 \times 10^{18} - 1.5 \times 10^{20} \text{ m}^{-3}$, which satisfies the operation conditions in Heliotron J. The laser has a Fabry-Pérot-type resonant cavity, which is comprised of a 3.2 m long, 56 mm diameter Pyrex tube and two plane reflectors. One of the reflectors is a plain mirror, and the other is a metal mesh with 90% reflectivity at the wavelength of the HCN laser.

author's e-mail: otani.yoshiaki.68r@st.kyoto-u.ac.jp

Two tungsten wires are placed in front of the laser aperture to determine the polarization of the laser. Helium gas and a mixed gas of CH₄ and N₂ are used in the discharge, and the ratio of these gasses is controlled to optimize the laser output power.

The interferometer is a Michelson type interferometer with a heterodyne detection system, as shown in Fig. 1. The laser is split into two beams. One beam is split again into a probe and a reference beam. The other beam is referred to as the local beam, and its frequency is shifted for heterodyne detection. We use a super rotating grating [7] as a frequency shifter, and the maximum frequency shift is 1.44 MHz. This enables the interferometer to achieve time resolution of less than 1 μs. The probe beam passes through the plasma mid-plane at an off-axis position of approximately $r/a \approx 0.35$. The reference beam is used to evaluate the phase shift. Both the probe and reference beams are mixed with the local beam by using Schottky barrier diode mixers, and the beat signals for both chords are detected. The beat signals are digitized at 10 MS/s with an analog-to-digital converter (YOKOGAWA WE7000). To determine the phase from the beat signal, the Hilbert transform [8] is used with a band pass filter between 0.9 MHz and 1.1 MHz so that phase changes occurring on time scales less than 10 μs are removed. In addition, unusually rapid phase change of 2π within 200 μs are considered a fringe jump and are removed. The phase data for both chords are compared, and the time trace of the line-integrated density is obtained.

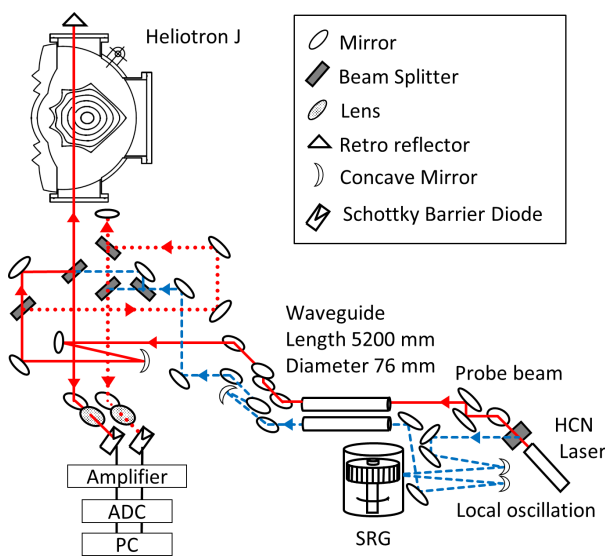


Fig. 1 Schematic of the FIR laser interferometer. Solid, dotted, and dashed lines denote the probe beam, reference beam, and local beam, respectively.

2.2 Estimation of the refraction of the FIR beam by high-density plasma using a ray-tracing code

Refraction of the probe beam cannot be ignored in the high density plasmas of Heliotron J. The displacement of the beam path due to refraction is estimated by using the TRAVIS ray-tracing code.

In this design, the probe beam, which is focused using a concave mirror located at $Z = -2.94$ m below the magnetic axis, is injected through a lower port of the vacuum chamber located at a major radius of $R_0 = 1.256$ m, as shown in Fig. 2 (a). The probe beam is then reflected by a retro reflector placed on the upper port, and is measured with a detector located at $Z = -3$ m.

Figure 2(b) show the results of a ray tracing calculation for a Heliotron J plasma parameterized by $n_e(\rho) = n_e(0)\{g + (1 - g)(1 - \rho^p)^q\}$, where $n_e(0) = 1.5 \times 10^{20} \text{ m}^{-3}$, $g = 0.053$, $p = 1.82$, and $q = 1.5$. The profile parameters are obtained by fitting a high-density plasma profile from Thomson scattering measurements. If a plane mirror is used as the reflector at the upper port, the beam displacement is estimated to be about 80 mm in the radial direction (coordinate R) at the detector position. In contrast, with a retro reflector the beam axis displacement is suppressed to less than 20 mm. In the toroidal direction (coordinate X), the displacement is less than 3 mm and is neglected. This shows that the retro reflector is necessary to compensate for beam refraction at high plasma density in Heliotron J.

The power loss caused by refraction is used to estimate the upper limit of the measurable plasma density. The HCN laser beam has a Gaussian intensity profile with a finite diameter, and the power loss cannot be determined

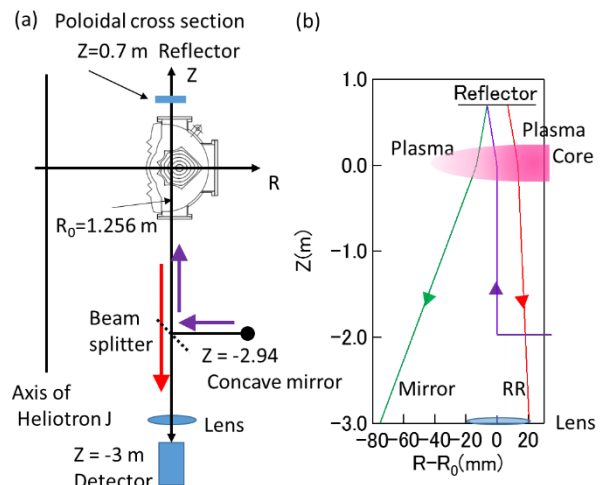


Fig. 2 (a) Coordinate system for ray tracing. (b) Comparison of the beam axis displacement at $n_e(0) = 1.5 \times 10^{20} \text{ m}^{-3}$ (fitted profile) between a plane mirror (mirror) and a retro reflector (RR). Purple line indicates the incident ray, red and green lines indicate the rays reflected by the plane mirror and the retro reflector, respectively.

by a calculation using only the central ray. We model the beam using five rays, as shown in Fig. 3 (a). The central ray, denoting the beam axis, is the yellow solid line marked by the square. The four peripheral rays are denoted by red dashed lines, and the circles represent the shape of the beam. The central and peripheral rays are aimed at the

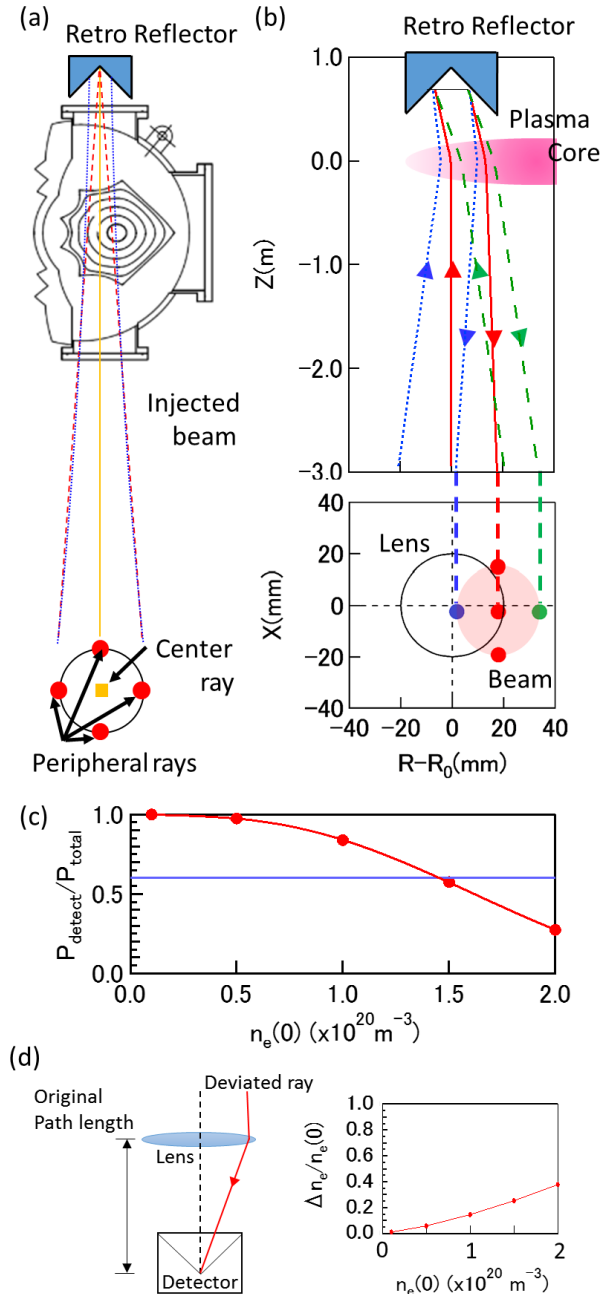


Fig. 3 (a) Assumption regarding the beam in ray tracing. (Above) Solid and dashed lines denote the ray traces. Dotted lines denote the propagation of the Gaussian beam. (Below) Composition of the Gaussian beam in the beam cross section. (b) Results of ray tracing. (c) Dependence of the detectable power on the density of plasma. (d) Left: Schematic to calculate the path length change owing to refraction. Right: Dependence of the error owing to the path length change on the density of plasma.

retro-reflector, where the beam waist of the Gaussian beam is located.

The displacement of the laser is shown in Fig. 3 (b). The propagation of the rays calculated for a peaked density profile with $n_e(0) = 1.5 \times 10^{20} \text{ m}^{-3}$ is shown in Fig. 3 (b) and Fig. 2 (b). The radial displacement in the R-direction is approximately 18 mm, and the displacement in the toroidal direction is less than 2.5 mm. The beam diameter decreases approximately 4% in the radial direction and increases approximately 2% in the toroidal direction due to the plasma refraction.

The calculated power loss and its density dependence are shown in Fig. 3 (c). The power incident on the detector is modeled by the overlapping area of the lens and the displaced beam. The beam shape shrinks in the R-direction and expands in the toroidal direction. The beam intensity profile is assumed to have a Gaussian shape, $I_{\text{beam}}(x, y) = I_0 \exp[-\{(R - R_0)/a\}^2 + (y/b)^2]$. I_0 is the intensity of the beam at the center, and a and b are the beam diameter in R and X directions, respectively. The ratio of detected power to total power, $P_{\text{detect}}/P_{\text{total}}$, is shown in Fig. 3 (c). The beam power decreases with plasma density; nevertheless, 60% of the launched power is detected at $1.5 \times 10^{20} \text{ m}^{-3}$. This loss is not significant on the measurement because the HCN laser output power of 40 mW at maximum and the minimum required power is about 4 mW for the detection.

The beam deviation caused by beam refraction results in the elongation of beam path length. The influence on the density measurement resulted from the path elongation is defined as Δn_e , and is evaluated as follows. The path length between the lens and the detector is extended approximately 1.3 mm for $n_e(0) = 1.0 \times 10^{20} \text{ m}^{-3}$, which correspond to a phase shift of approximately 8π , for a plasma density change of $\Delta n_e/n_e(0) \approx 0.15$. The density dependence of the path elongation effect is summarized in Fig. 3 (d). In addition, the phase shift in plasma is negligible because the path length is extended 27 μm even in the case of $n_e(0) = 1.0 \times 10^{20} \text{ m}^{-3}$. This result indicates that the path length change due to beam deviation should be considered, especially in the case of the high density plasma realized by SMBI and HIGP.

In the case of the microwave interferometer, the beam deviation is more than 90 mm for $n_e(0) = 5 \times 10^{19} \text{ m}^{-3}$, which is larger than the port in the Heliotron J vacuum chamber. Here, the interferometer, which has a vertical viewing chord passing through the center of plasma, utilizes a 130 GHz microwave beam that cut-off is at a plasma density of $1 \times 10^{20} \text{ m}^{-3}$. This system cannot be applied to the measurement of electron density higher than $5 \times 10^{19} \text{ m}^{-3}$ [3]. The refraction effect on the plasma for the microwave is less than 1.18 mm in the case of $n_e(0) = 2.0 \times 10^{19} \text{ m}^{-3}$, which induces 1.5π radians corresponding to Δn_e of $1.3 \times 10^{17} \text{ m}^{-3}$. This error is larger than the error of the FIR system but is negligible for the plasma with the density of $n_e(0) < 2.0 \times 10^{19} \text{ m}^{-3}$ discussed in this paper.

3. Experimental Result and Discussion

A new FIR interferometer has been constructed and used to make measurements of the Heliotron J plasma. Experiments with plasma heating by NBI, as well as a combination of ECH and NBI, are conducted and the typical waveforms for the plasma line-averaged density measured by the microwave interferometer (\bar{n}_e^{MICRO}), the plasma stored energy measured by a diamagnetic loop, and the heating patterns are shown in Figs. 4 (a), 4 (b), and 4 (c), respectively. Responses less than $10\mu\text{s}$ are eliminated from the interferometer signal by digital band-pass filtering (0.9 - 1.1 MHz). In addition, the density resolution depends on the optical vibration and is less than $0.2 \times 10^{19} \text{ m}^{-3}$. The first line-averaged density data obtained with the new FIR interferometer (\bar{n}_e^{FIR}) are shown in Fig. 4 (d). The data contains noise, which comes from changes in the coil current of Heliotron J. The noise can be reduced by increasing the laser power and increasing the signal-to-noise ratio. The error owing to the path length change in the FIR laser interferometer is about 1%, and it is negligible compared with the noise of 3 - 4%. In contrast, the error of the microwave interferometer owing to the path length change is less than 1% in this density region and is negligibly small.

The two measurements are different because the viewing chords are located at different toroidal cross section, and one is shifted from the center of the plasma axis. Because the measured value of the FIR interferometer is higher than that of the microwave interferometer, the density profile is inferred to have a hollow shape. The plasma density profile measured by Thomson scattering is modeled by Eq. (1). The fit,

$$n_e(\rho) \propto \left\{ 1 - \left(\frac{\rho}{1.2} \right)^2 \right\}^4 \left\{ 1 - (0.6 + 0.4H) \exp\left(-\frac{\rho^2}{3}\right) \right\} \equiv f(\rho), \quad (1)$$

is shown in Fig. 5 (a), where ρ and H are the normalized radius and parameter indicating the degree of profile hollowness, respectively. The local plasma density along these chords is shown as a function of the vertical coordinate Z in Fig. 5 (b). Using Eq. (1) and considering the chord differences, the ratio of the line-averaged density along each

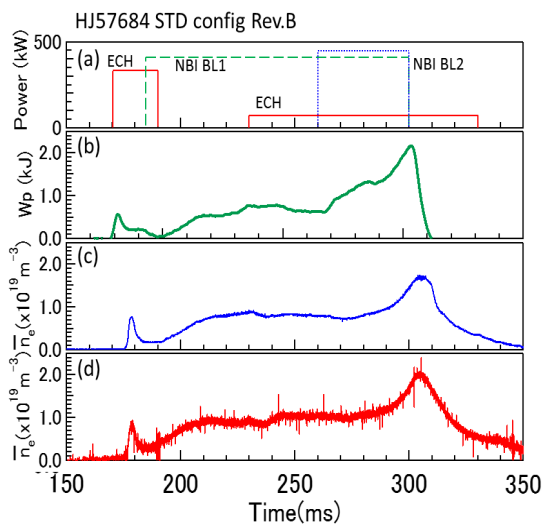


Fig. 4 Time trace of (a) the heating power of ECH and NBI, (b) stored energy (Wp), (c) \bar{n}_e^{MICRO} , and (d) \bar{n}_e^{FIR} .

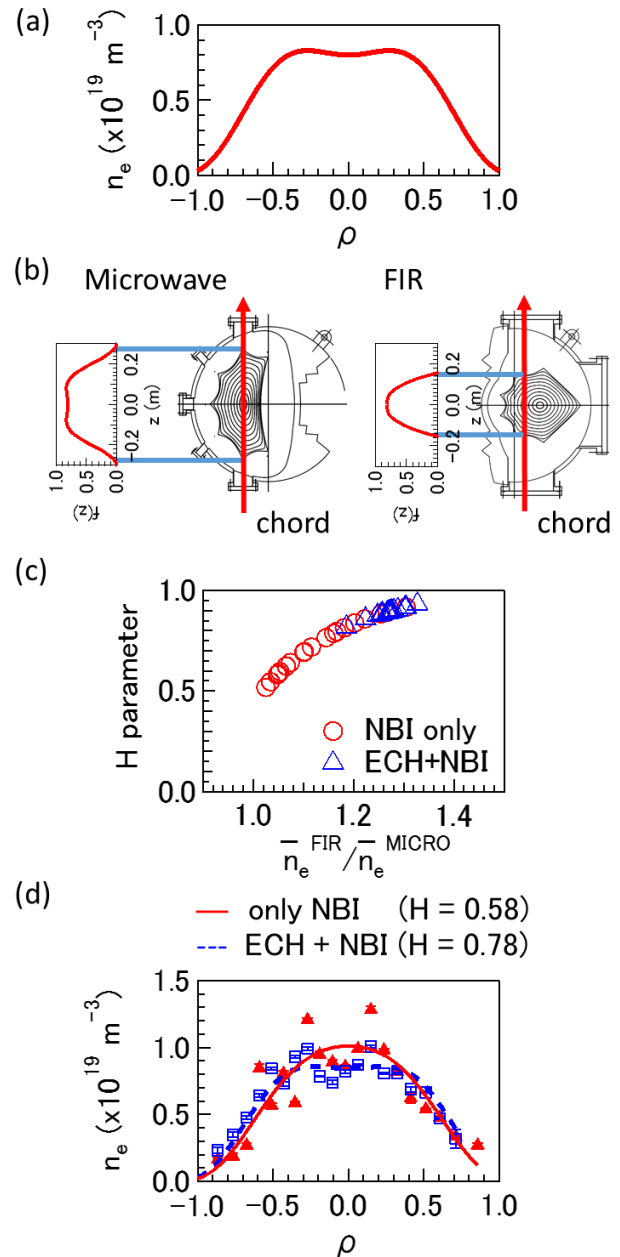


Fig. 5 (a) Typical hollow density profile produced in Heliotron J. (b) Chord difference between microwave and FIR laser interferometer. (c) (red circles) H parameter in the NBI-only plasma (210 - 230 ms); (blue triangles) H parameter in the ECH + NBI plasma (240 - 260 ms) (d) Density profile from the Thomson scattering measurements.

chord for both interferometers ($\bar{n}_e^{\text{FIR}}/\bar{n}_e^{\text{MICRO}}$) was calculated for varying degree of hollowness, the H parameter, and then the relation between H and $\bar{n}_e^{\text{FIR}}/\bar{n}_e^{\text{MICRO}}$ was calculated.

The ratio $\bar{n}_e^{\text{FIR}}/\bar{n}_e^{\text{MICRO}}$ is also calculated from the experimental data, and the resulting H parameter is shown by the red circles and blue triangles in Fig. 5 (c). The red circles indicate the H parameter of the NBI plasma from 210 - 230 ms, and the blue triangles indicate the H parameter of the ECH + NBI plasma from 240 - 260 ms. The H parameter of the ECH + NBI plasma is higher than that of the NBI heated plasma. The H parameter obtained with the interferometers indicates that the profile shape of the ECH + NBI plasma is flatter than that of NBI plasma. Figure 5 (d) shows the Thomson scattering measurements and the fitted curve. The open squares and solid triangles denote the local density of the NBI heated plasma between 210 ms and 230 ms, and the ECH + NBI plasma between 240 ms and 260 ms, respectively. The dashed and the solid lines are the corresponding fitted curves. The plasma density profile of the ECH + NBI plasma between 240 - 260 ms is flatter than that of NBI plasma between 210 - 230 ms, which is consistent with interferometer observations.

4. Summary

A new FIR laser interferometer with high time resolution has been developed in Heliotron J. The 1 MHz intermediate frequency for heterodyne detection is obtained using a super rotating grating. A resolution of less than 1 μm is also achieved. Beam refraction can be significant in Heliotron J; however, ray tracing calculation indicate that the retro reflector installed in Heliotron J can sufficiently compensate for the maximum beam deviation expected in Heliotron J, near a line-averaged plasma density of $n_e(0) = 1.5 \times 10^{20} \text{ m}^{-3}$. Ray tracing calculation indicate

that the power loss due to beam refraction is approximately 40% at $n_e(0) = 1.5 \times 10^{20} \text{ m}^{-3}$ in both cases of the fitted density profile.

Line-averaged plasma density measurements with the new FIR laser interferometer have been successfully obtained. Due to viewing chord differences, \bar{n}_e^{FIR} is different from \bar{n}_e^{MICRO} . By making assumptions about the plasma density profile, the profile hollowness can be estimated from the ratio $\bar{n}_e^{\text{FIR}}/\bar{n}_e^{\text{MICRO}}$ with high time resolution in Heliotron J. The plasma density profile of the ECH + NBI plasma is higher than that of the NBI heated plasma, and this result is consistent with Thomson scattering measurements. This technique is valuable for plasma transport analysis and can be used to study changes in the confinement with advanced fueling techniques, such as SMBI and HIGP.

Acknowledgments

The authors are grateful to the Heliotron J supporting group for the excellent arrangement of the experiments. This study was performed with the support and under the auspices of the Collaboration Program of the Laboratory for Complex Energy Processes, Institute of Advanced Energy, Kyoto University and the NIFS Collaborative Research Program (NIFS10KUHL030, NIFS09KUHL028 and NIFS13KUHL056).

- [1] N. Ohyabu *et al.*, Phys. Rev. Lett. **97**, 055002 (2006).
- [2] O. Kaneko *et al.*, Plasma Fusion Res. **4**, 027 (2009).
- [3] T. Mizuuchi *et al.*, J. Nucl. Mater. **415**, 443 (2011).
- [4] S. Kobayashi *et al.*, 40th EPS Conf., 1-5 July (2013) P1.148.
- [5] N.B. Marushchenko *et al.*, Comput. Phys. Commun. **185**, 165 (2014).
- [6] D. Véron *et al.*, Opt. Soc. Am. **67**, 964 (1977).
- [7] T. Maekawa *et al.*, Rev. Sci. Instrum. **62**, 304 (1991).
- [8] S. Ohshima *et al.*, Rev. Sci. Instrum. **85**, 11E814 (2014).